Materials Research Express

PAPER

Influence of the order of boron and phosphorus diffusion on the fabrication of thin bifacial silicon solar cells

To cite this article: Vanessa da Conceição Osório *et al* 2016 *Mater. Res. Express* **3** 105022

View the article online for updates and enhancements.

You may also like

- Development of high-efficiency bifacial photovoltaic module and simulation method for its power generation
Takahiro Nakamura, Syuji Fukumochi, Yu Maruyama et al.
- Bifacial dye-sensitized solar cells utilizing green-colored NIR sensitive unsymmetrical squaraine dye
Suraya Shaban, Pritha Roy, Ajendra Kumar Vats et al.
- Optimization of various terminal topologies of bifacial perovskite/$FeSi_2$ tandem solar cell
Usama Bin Qasim, Muhammad Mohsin Saeed and Hassan Imran

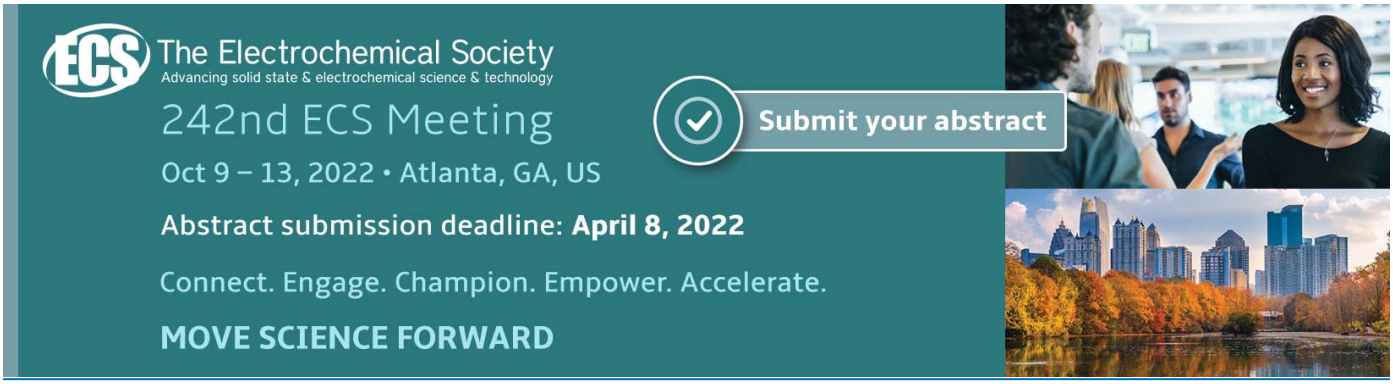

This content was downloaded from IP address 201.54.143.84 on 30/03/2022 at 13:41

Materials Research Express

RECEIVED
18 August 2016

ACCEPTED FOR PUBLICATION
13 September 2016

PUBLISHED
13 October 2016

PAPER

Influence of the order of boron and phosphorus diffusion on the fabrication of thin bifacial silicon solar cells

Vanessa da Conceição Osório, Adriano Moehlecke and Izete Zanesco

Solar Technology Nucleous, Pontifical Catholic University of Rio Grande do Sul, Av. Ipiranga, 6681, P.96A, 90619-900, Porto Alegre, RS, Brazil

E-mail: moehleck@pucrs.br

Keywords: silicon solar cells, bifacial solar cells, thin silicon wafers, selective BSF

Abstract

The aim of this paper is to analyze the fabrication process of thin bifacial silicon solar cells concerning the order of diffusions to form p^+ and n^+ regions. The n^+pp^+ structure with the p^+ selective region was implemented by using thin solar grade Czochralski silicon wafers. The whole rear face was doped with boron deposited by spin-on and thermally diffused and an Al metal grid was screen-printed and diffused. The phosphorus diffusion after the boron one produced the thinner n^+ emitter and thinner dead layer, which allow the manufacturing of more efficient solar cells. Furthermore, the phosphorus diffusion at the end of processing promoted gettering, enhancing the minority charge carrier lifetime. Solar cells with the phosphorus diffusion after the boron one reached front and rear efficiencies of 14.0% and 10.4%, respectively, without any surface passivation.

1. Introduction

The current market for PV modules is dominated by the crystalline silicon solar cells and the silicon wafer represents the order of 42% of the final value of the photovoltaic module [1]. Therefore, the reduction in thickness and thus the amount of crystalline material used is critical to reduce the production cost of these devices. Nowadays, silicon wafers have a thickness of around 180 μm and research efforts have been made to obtain devices in 120 μm thick wafers [2, 3]. However, for cost reduction, the conversion efficiency of the devices should be maintained and, for this, must be developed processes to optimize the light trapping and to decrease the recombination on the rear face. Similarly, the production yield should be above 90% [4], which is a challenge from a technical point of view.

The bifacial solar cell is capable of converting solar radiation into electrical energy that reaches on both faces of the device. This device has been studied since the 1960 years [5, 6] and it can be used in solar concentrators or photovoltaic modules that receive the solar radiation reflected by the surfaces under the modules [7–10]. Yang *et al* developed bifacial n^+pp^+ cells of large area (pseudo-square of 156 mm $\times$ 156 mm) and they obtained efficiencies of 16.6%/12.8% for n^+ face/p^+ face illumination, by using Cz (Czochralski) monocrystalline silicon wafers, p-type, 200 μm thick, with homogenous n^+ and p^+ regions produced by diffusions based on $POCl_3$ and BBr_3, respectively, and screen-printed metal grid [11]. Similar devices, but with smaller Si wafers, 125 mm $\times$ 125 mm, were reported by Duran *et al* [12], achieving efficiencies of 17.3% and 15.3% when the device was illuminated by n^+ face (front) and p^+ face (rear), respectively. Also, using silicon Cz p-type wafers, Janβen *et al* [13] manufactured bifacial solar cells that reached the efficiencies of 17%/10.3% (front/rear illumination). Unlike the device presented by Yang *et al* [11] and Duran *et al* [12], in the work of Janβen and collaborators [13], boron was not diffused in the rear face and a n^+p structure was obtained. The front and rear surfaces were coated with a passivating thin film of a-SiN_x:H. The solar cell metal grid was deposited by screen-printing on both faces. The rear face received an Al metal grid, producing the effect of back surface field (BSF).

The combination of thin wafers and bifacial structures can reduce the photovoltaic electricity cost because it decreases the consumption of silicon and allows the illumination of the rear face. In addition, the reduced

© 2016 IOP Publishing Ltd

thickness allows the use of lower quality silicon taking into account that the minority charge carriers generated by solar radiation on rear face have a shorter path to reach the pn junction.

By using FZ (*float zone*) silicon, 130 μm thick, bifacial cells achieved the efficiency of 16.9% and 10.4% for illumination by n^+ and p^+ face, respectively [14]. The BSF region was produced by deposition of a boron rich paste followed by a diffusion in a belt furnace. However, the devices had reduced area (4 cm^2) and metal grids obtained by high vacuum evaporation were used, a process uneconomical in the current solar cell industry. The authors also used phosphorus and boron pastes deposited by screen-printing in order to obtain n^+ and p^+ regions after firing, but efficiencies achieved were lower: 11.6%/10.8%. Recart [15] developed bifacial devices on larger area (24.7 cm^2) in Cz-Si wafers 120 μm thick. The n^+ emitter was obtained by P diffusion ($POCl_3$ as source) and the p^+ region, in the rear face, was produced by deposition of boron rich pastes and diffusion in a belt furnace. The n^+pp^+ solar cells with homogeneous n^+ and p^+ regions reached the efficiencies of 14.3% and 10.8%, for front (n^+) and rear (p^+) illumination, respectively [15]. However, the busbars were not considered in the metal grid shadowing because it remained outside of the active area. Steckemetz *et al* [16] have studied the n^+p structure with front and rear surfaces passivated with SiN_x and with Al BSF localized only under the electrical contacts in the rear face. The efficiencies of 14.6%/13.6% for front/rear illumination were obtained on devices of reduced area (4 cm^2) and with Si-Cz wafers of 140 μm thick [16]. However, bifacial silicon solar cells were not developed in solar grade Cz-Si and with boron diffusion based on spin-on deposition.

The aim of this paper is to present the development of thin bifacial solar cells with n^+pp^+ structure and selective p^+ region processed in solar grade Cz-Si. The selective emitter was performed by boron diffusion based on spin-on deposition on the rear face and on Al grid screen-printed and fired. The order of the boron and phosphorus diffusion in the process sequence was analyzed.

2. Materials and methods

For this study, we used solar grade silicon wafers grown by the Czochralski method, p-type, boron doped, resistivity of 2 Ω cm, ⟨100⟩ orientation. The thickness of the wafers was reduced to approximately 145 μm by a chemical etch based on KOH and deionized water (H_2O_{DI}). This solution was employed because there was no market availability of thin wafers.

To analyze the order of boron and phosphorus diffusions in the manufacture of thin n^+pp^+ bifacial solar cells, two processes were developed, called α and β. The steps of the fabrication sequence α and β are depicted in figure 1. In the process α, the boron was deposited after the diffusion of phosphorus and, in the process β, before the diffusion of phosphorus. In the former, boron depletion due to the impurity segregation to the oxide layer is avoided, but n^+ region will be thicker. Otherwise, process β will produce thinner phosphorus emitters, but boron depletion near the surface can enhance the contact resistance and surface recombination. The baseline structure obtained is presented in figure 2.

In both processes, the anisotropic etch in a bath of KOH, isopropyl alcohol and H_2O_{DI} was performed to form micropyramids. After this process, the wafers were cleaned in the standard RCA solution [17].

In the process α, after cleaning, the wafers were introduced in a high temperature furnace (at 1000 °C) to grow an oxide layer on the surfaces. The silicon dioxide formed has the purpose of protecting one of the faces of the wafers during the thermal diffusion of phosphorus. A photoresist was deposited by spin-on in one of the faces and after the resist drying, the oxide layer on the other side was extracted with a solution of buffered HF. The resist was removed by acetone and wafers were cleaned with RCA solution.

For formation of n^+ region, phosphorus was diffused in a quartz tube by using $POCl_3$ as source. The phosphorus diffusion was carried out at 875 °C for 60 min followed by a drive-in for 60 min. After that, phosphorus silicate glass was etched away by means of a hydrofluoric acid solution.

A liquid containing boron (PBF20, Filmtronics) was spun-on on the undoped face and the wafers were introduced in an oven for evaporation of solvents. Boron was diffused into the silicon wafers in a quartz tube furnace at 1000 °C during 20 min. This kind of doping has been studied since the 1970 years [18] for microelectronic industry and also had been proposed to produce n-type silicon solar cells as a substitute of most commonly used BBr_3. This source of boron doping need safety precautions and can degrade the minority charge carrier lifetime through the formation of a boron rich layer (BRL) [19]. Singha and Solanki also observed the formation of BRL after boron spin-on and diffusion, but they reported that controlled diffusion processes and oxidation can partially reduce the BRL thickness and improve the minority carrier lifetime by more than 10% [20].

The process β differed from previous by the order of the boron diffusion within the process sequence. In addition, the layer of borosilicate glass formed during the diffusion of boron was used to protect one face of the diffusion of phosphorus. Consequently, the β process requires fewer steps than the α one, avoiding a thermal oxidation step and a chemical cleaning [21]. The parameters used for the diffusion of boron were the same used

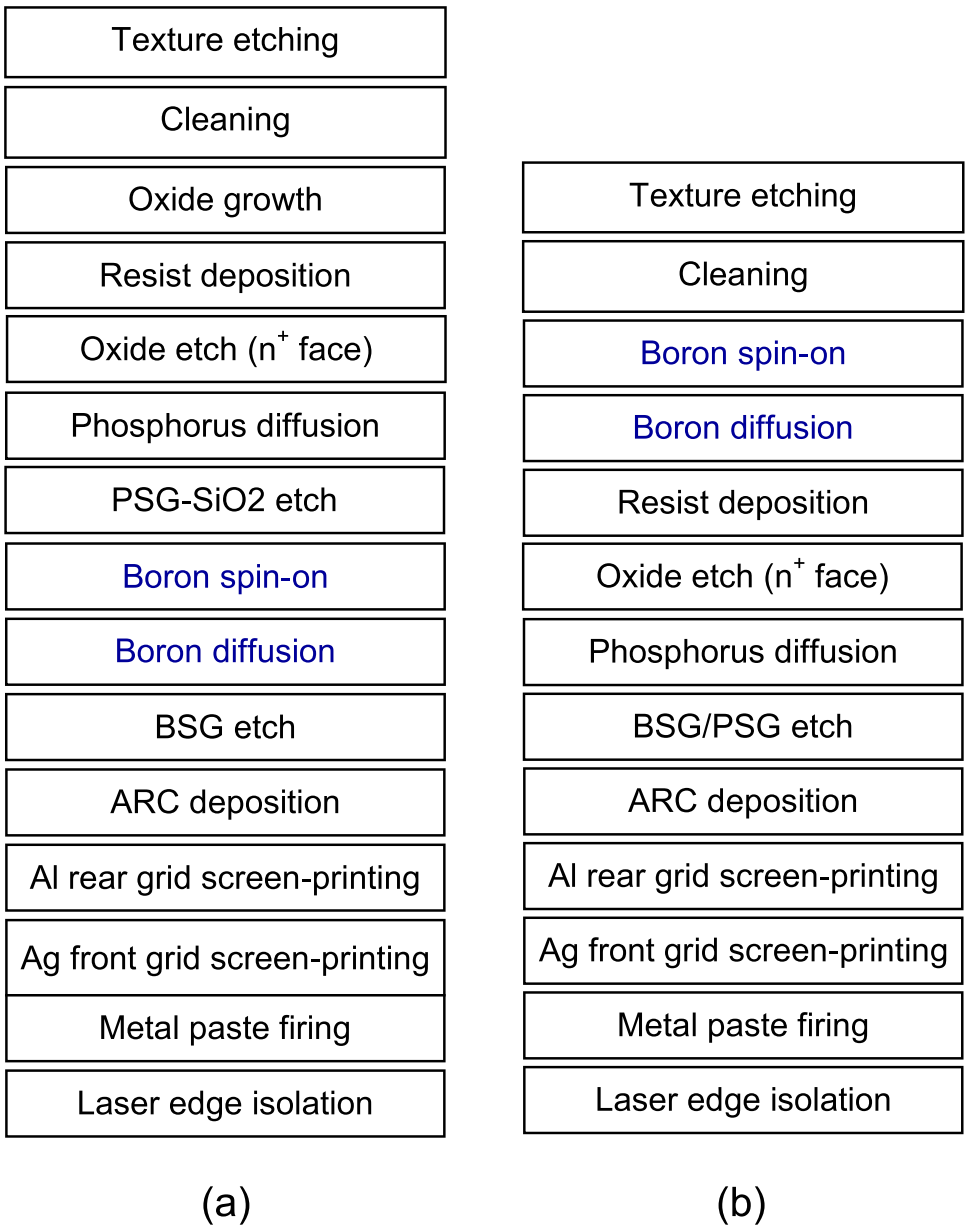

Figure 1. Fabrication processes sequence of the bifacial solar cells: (a) α, with phosphorus diffusion in the first step of the process and (b) β, with P diffusion after B one.

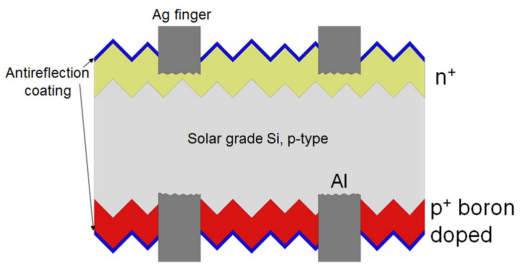

Figure 2. Thin bifacial solar cell with selective BSF doped with Al and B.

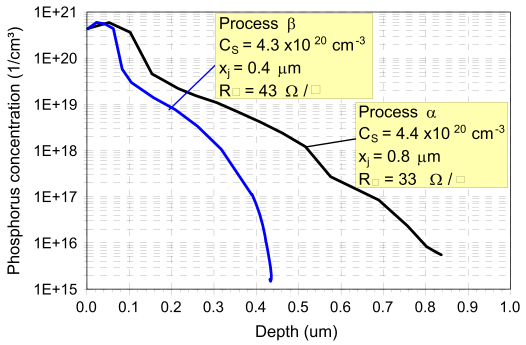

Figure 3. Phosphorus doping profiles obtained by ECV.

in the process α. For the phosphorus diffusion, the pre-deposition time was the same, but the drive-in step was reduced to 10 min, allowing the production of a thinner n^+ emitter.

The boron and phosphorus doped regions were characterized by measuring the sheet resistance ($R_\square$) by four-point probe technique and by obtaining the impurity profile by the ECV technique (electrochemical capacitance–voltage profiling) [22, 23]. The $R_\square$ was measured in 13 regions in the doped wafer. The thickness of the n^+ region (x_j) and p^+ one (x_{BSF}) as well as the surface impurity concentration (C_S) were obtained from the impurity profile.

In both processes, after the diffusion, oxides were etched-off and an RCA was performed. Surface passivation based on SiN_x or SiO_2 were not used in the devices. The TiO_2 antireflection coating (ARC) was deposited by high vacuum evaporation with e-beam. Although the bifacial cells have to be an ARC on both faces, we preferred to deposit ARC only on the front face in order to optimize the temperature of the aluminum diffusion, avoiding the etched-through process of the ARC by Al metal grid.

The rear metal grid based on PV381 (DuPont) was screen-printed and this grid has the double function: to contact the silicon wafer and produce the selective BSF region. In the non-metal covered regions on the rear face, the BSF effect is produced by boron doped region previously diffused. The boron and aluminum doped regions generate an electric field that repels the minority carrier lifetime, reducing the surface recombination velocity in the rear face. The front grid was formed by screen-printing a silver paste. The pastes were dried in a belt furnace and they were fired at 840 °C. During the firing process, the silver paste etches-through the ARC and contact electrically the n^+ doped region and the Al formed the selective BSF region. After the metal grid deposition, edge isolation was performed with a laser equipment.

All the devices were characterized under standard conditions (100 mW cm^{-2}, AM1.5G and 25 °C) in a solar simulator calibrated with silicon solar cells previously measured at CalLab—FhG-ISE (*Fraunhofer-Institut für Solare Energiesysteme*), Germany. Cells had area of 61.58 cm^2 (pseudo-square of 800 mm × 800 mm) with a standard two-busbars. More efficient solar cells were analyzed by light beam induced current technique (LBIC) [24] in four wavelengths: 648, 845, 953 and 973 nm and the minority carrier diffusion length (L_D) was estimated.

3. Results and discussion

The phosphorus doped regions presented average sheet resistance of (33 ± 2) Ω/□ and (43 ± 2) Ω/□ following processes α and β, respectively. The figure 3 shows the phosphorus doping profiles. The surface impurity concentration was similar for wafers processed by both fabrication sequences of about 4.4×10^{20} cm^{-3}. But the thickness of the n^+ emitter (or the pn junction depth) obtained with the process α was twice the value obtained by process β. Moreover, the change of the sequence of the diffusions and the reduction of the drive-in time for phosphorus diffusion diminished the thickness of the dead layer, i.e., the region with high impurity concentration and, consequently, the high recombination.

The boron diffusion before the phosphorus one in the process β produced a 0.2 μm thicker p^+ region. But sheet resistances observed were similar, as figure 4 shows. The thinner p^+ region with higher C_s corresponding to the device processed with the fabrication sequence α could be better, allowing higher short-circuit currents when the solar cell is illuminated by p^+ doped face. Nevertheless, as we will show, other factors, like the minority carrier lifetime, will be most important.

Average electrical characteristics of the solar cells are depicted in the table 1. Measurements of open-circuit voltage (V_{OC}), short-circuit current density (J_{SC}), fill factor (FF) and efficiency (η) were obtained for two independent illumination modes: by p^+ and n^+ region.

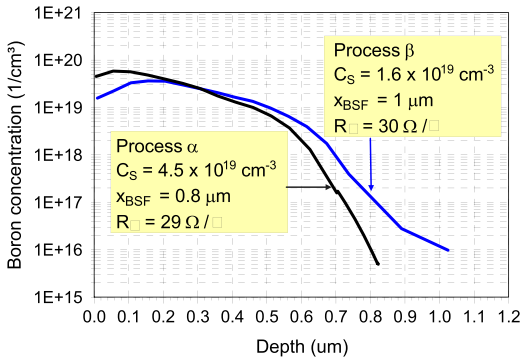

Figure 4. Boron impurity concentration obtained by ECV and characteristics of the doped regions.

Table 1. Average electrical parameters of the solar cells manufactured by processes α e β.

Front illumination (by n^+ face)				
Process	V_{OC} (mV)	J_{SC} (mA cm^{-2})	FF	η(%)
A	586 ± 1	27.0 ± 1,0	0.71 ± 0,01	11.2 ± 0,4
B	591 ± 17	31.6 ± 1.0	0.71 ± 0.01	13.4 ± 1.0
Rear illumination (by p^+ face)				
A	579 ± 3	18.0 ± 1.0	0.72 ± 0.01	7.6 ± 0.4
B	582 ± 18	20.6 ± 2.6	0.73 ± 0.01	8.8 ± 1.5

Table 2. Electrical characteristics of the best bifacial solar cells obtained by processes α and β and results from simulation by means of the PC1D device-modeling program.

Process	Parameters fitted by simulation	Ilum.	Results	V_{OC} (mV)	J_{SC} (mA cm^{-2})	FF	η (%)
α	$S_f = 1 \times 10^7$ cm s^{-1}	n^+	Experimental	586	27.5	0.722	11.6
	$S_p = 1 \times 10^7$ cm s^{-1}		Simulated	588	30.0	0.680	12.0
	$\tau = 9$ μs	p^+	Experimental	576	17.5	0.729	7.4
	$r_S^* = 3{,}2$ Ω cm^2		Simulated	575	17.0	0.720	7.1
β	$S_f = 1 \times 10^7$ cm s^{-1}	n^+	Experimental	602	32.3	0.719	14.0
	$S_p = 1 \times 10^7$ cm s^{-1}		Simulated	602	32.6	0.713	14.0
	$\tau = 55$ μs	p^+	Experimental	594	22.2	0.739	9.7
	$r_S^* = 2{,}4$ Ω cm^2		Simulated	592	22.1	0.749	9.8

The devices fabricated with process β and illuminated by n^+ face presented higher V_{OC}, J_{SC} and η than that fabricated with process α. The J_{SC} was the key parameter that explained that the efficiency of devices processed by sequence β reached efficiencies 2.2% (absolutes) higher than those manufactured by sequence α. With illumination by p^+ face, the cells obtained by sequence β also showed an enhancement of the V_{OC} and J_{SC} of 3 mV and 2.6 mA cm^{-2}, respectively. For both processes, the fill factor of the solar cells was low, indicating a high series resistance. The low J_{SC} of the cells illuminated by BSF is partially due that no ARC was deposited on the rear face.

Table 2 summarizes the electrical characteristics of the best solar cells produced with selective B/Al BSF. In order to assess the values of the effective minority carrier lifetime (τ), front surface recombination velocity (S_f), rear surface recombination velocity (S_r) and specific series resistance (r_s), the bifacial cells were simulated by using the PC1D computer program [25] and these parameters were adjusted to fit in well the simulated V_{OC}, J_{SC}, FF and η to the experimental ones. The following parameters were used to simulate the solar cells: wafer thickness of 145 μm, reflectance of a textured surface covered with ARC, metal grid shadowing factor of 9.5% and base resistivity of 2 Ω cm. Impurity profiles were adjusted in the PC-1D to fit the experimental ones presented in figures 3 and 4.

The values of the surface recombination velocity are according to the absence of surface passivation, but the minority carrier lifetime of 9 μs is low for cells made with the process α. On the other hand, the solar cells with

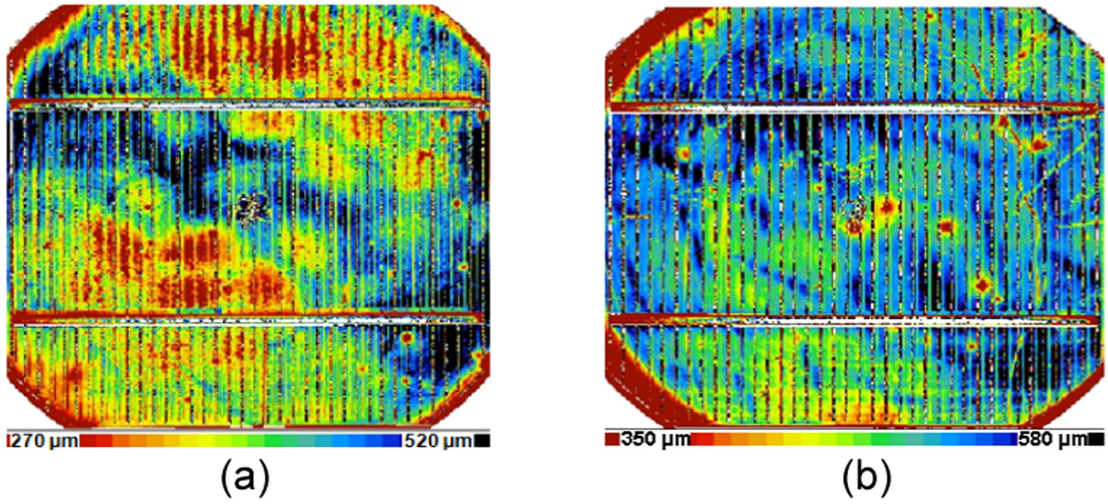

Figure 5. Two-dimensional distribution of the minority carrier diffusion length of the solar cells fabricated with the process α (a) ($L_{DAverage} = 390\ \mu m$) and with the process β (b) ($L_{DAverage} = 510\ \mu m$).

the diffusion of phosphorus at the end of the process presented $\tau = 55\ \mu s$. This higher bulk lifetime for solar grade silicon is due to the gettering mechanisms provided by diffusion of phosphorus at the end of the processing [26]. This way, the small thickness of the n^+ region and the high minority carrier lifetime observed in solar cells processed by sequence β explain the higher J_{SC}, V_{OC} and η. The series resistance was high for all the solar cells and is not associated with the order of the B/P diffusions, but it is related to the rear metal grid. On the rear p^+ face, an aluminum metal grid was screen-printed and this metal paste presents a resistivity higher (twice) than the silver paste used on the n^+ face.

More efficient solar cells were processed with the sequence β and reached the efficiency of 14% for illumination by the face n^+ and 9.7% for illumination by the face p^+. A TiO_2 ARC was deposited on the rear face and J_{SC} increased by 2 mA cm^{-2} and, consequently, efficiency rose to 10.4%. The results are similar to those published by Recart [15], but in this work we produce larger devices in solar grade Si-Cz, spin-on dopant was used and the busbar was inside active area, the typical approach of industrial devices. The implementation of surface passivation by thermally grown SiO_2 can reduce the S for values of around 4.3×10^4 cm s^{-1} (to $C_s = 4.3 \times 10^{20}$ cm^{-3}) [27] and 5.5×10^4 cm s^{-1} (to $C_s = 1.6 \times 10^{19}$ cm^{-3}) [28, 29], for n^+ and p^+ doped faces of textured silicon wafers, respectively. The surface passivation and a reduction of specific series resistance to values lower than 1 Ω cm^2 can enhance the efficiency to about 16.7% for front (n^+) illumination and to 13.1% for rear illumination (p^+), efficiencies similar to that obtained by Yang *et al* [11] with thicker wafers.

The figure 5 illustrates the distribution of the minority carrier diffusion length obtained by the LBIC technique of the more efficient devices manufactured with α and β sequences. The β process provided a more uniform distribution of L_D, with a larger region of diffusion lengths close to the maximum value. The device processed with the sequence α shows an average value of the diffusion length ($L_{DAverage}$) of about 390 μm. The solar cell fabricated with β sequence achieved $L_{DAverage} = 510\ \mu m$. Taking into account a same diffusion coefficient (D) for minority carriers and the values of τ presented in the table 2, the estimated L_D were 164 μm ($\tau = 9\ \mu s$) and 404 μm ($\tau = 55\ \mu s$) for devices processed by fabrication sequences α and β. The difference between the values of L_D obtained by simulating the solar cells with the PC1D program and obtained by LBIC technique is due to the fact that the LBIC technique evaluates the substrate and also the effectiveness of the BSF. The PC1D also evaluates the effect of BSF, but isolates the phenomena of recombination in the substrate and on the surface.

4. Conclusions

Two processes have been developed to manufacture thin bifacial solar cells with the selective BSF region, formed by diffusion of boron and aluminum. Boron was deposited by spin-on and diffused in an open tube quartz furnace and Al grid was screen-printed and diffused in a belt furnace. In the process α, the diffusion of boron was performed at the end of the process and in the process β, the diffusion of phosphorus was implemented after the diffusion of boron.

In the process β, n^+ emitter presented a lower depth and a thinner 'dead layer' was formed, decreasing recombination in this region and increasing minority short-circuit current of the solar cells when compared to

those fabricated with the process α. In addition, the diffusion of phosphorus after the boron one produced bifacial solar cells with longer minority carrier lifetime and diffusion length, resulting in an increase in efficiency when the solar cells were illuminated by the selective boron/aluminum BSF. Therefore, to manufacture bifacial solar cells in solar grade thin silicon wafer, the diffusion of phosphorus should be held at the end of the processing.

Acknowledgments

The authors acknowledge the financial support provided by state utility CEEE-D and by the Brazilian financing agencies FINEP and CNPq.

References

[1] Goodrich A, Hacke P, Wang Q, Sopori B, Margolis R, James T L and Woodhouse M 2013 A wafer-based monocrystalline silicon photovoltaics road map: utilizing known technology improvement opportunities for further reductions in manufacturing costs *Sol. Energy Mater. Sol. Cells* **114** 110–35
[2] Beaucarne G *et al* 2006 Thin, thinner, thinnest: an evolutionary vision of crystalline Si technology *Proc. 21st European Photovoltaic Solar Energy Conf. and Exhibition* pp 554–9
[3] Upadhyaya A, Sheoran M, Ristow A, Rohatgi A, Narayanan S and Roncin S 2006 Greater than 16% efficient screen printed solar cells on 115–170 μm thick cast multicrystalline silicon *Conf. Record of the 4rd IEEE World Conf. on Photovoltaic Energy Conversion* pp 1052–5
[4] Hogan S J 1998 Silicon one sun, terrestrial modules *Solar Cells and Their Applications* ed L D Partain (New York: Wiley) pp 213–21
[5] Cuevas A 2005 The early history of bifacial solar cells *Proc. 20th European Photovoltaic Solar Energy Conf. and Exhibition* pp 801–5
[6] Coello J, Cañizo C and Luque A 2006 Review on bifacial solar cell structures for industrialization *Proc. 21st European Photovoltaic Solar Energy Conf. and Exhibition* pp 1358–61
[7] Cuevas A, Luque A, Eguren J and Alamo J 1982 50% more output power from an albedo-collecting flat panel using bifacial solar cells *Sol. Energy* **19** 419–20
[8] Zanesco I and Lorenzo E 2002 Optimisation of an asymmetric static concentrator: the PEC-44D *Prog. Photovolt., Res. Appl.* **10** 361–76
[9] Moehlecke A, Febras F S and Zanesco I 2013 Electrical performance analysis of PV modules with bifacial silicon solar cells and white diffuse reflectors *Sol. Energy* **96** 253–62
[10] Appelbaum J 2016 Bifacial photovoltaic panels field *Renew. Energy* **85** 338–43
[11] Yang L, Ye Q H, Ebong A, Song W T, Zhang G J, Wang J X and Ma Y 2011 High efficiency screen printed bifacial solar cells on monocrystalline Cz silicon *Prog. Photovolt., Res. Appl.* **19** 275–9
[12] Duran C, Buck R, Kopecek R, Libal J and Traverso F 2010 Bifacial solar cells with boron back surface field *Proc. 25th European Photovoltaic Solar Energy Conf. and Exhibition* pp 2348–52
[13] Janβen L, Windgassen H, Bätzner D L, Bitnar B and Neuhaus H 2009 Silicon nitride passivated bifacial Cz-silicon solar cells *Sol. Energy Mater. Sol. Cells* **93** 1435–9
[14] Pérez L, Coello J, Freire I, Varner K, Lago R, Bueno G, Cañizo C and Luque A 2005 Global processes for the fabrication of low cost bifacial solar cells *Proc. 20th European Photovoltaic Solar Energy Conf. and Exhibition* pp 891–4
[15] Recart F 2001 Evaluation of screen-printing as metallization technology for efficient solar cells *Doctor Thesis* University of the Basque Country, Spain
[16] Steckemetz S, Metz A and Hezel R 2001 Thin Cz-silicon solar cells with rear silicon nitride passivation and screen printed contacts *Proc. 21st European Photovoltaic Solar Energy Conf. and Exhibition* pp 1902–6
[17] Kern W 1998 *Handbook of Semiconductor Wafer Cleaning Technology* (New Jersey: Noyes Publications) 623p
[18] Becker J A 1974 Silicon wafer processing by application of spun-on doped and undoped silica layers *Solid-State Electron.* **17** 87–94
[19] Kessler M, Ohrdes T, Wolpensinger B and Harder N P 2010 Charge carrier lifetime degradation in Cz silicon through the formation of a boron-rich layer during BBr_3 diffusion processes *Semicond. Sci. Technol.* **25** 1–9
[20] Singha B and Solanki C S 2016 Impact of a boron rich layer on minority carrier lifetime degradation in boron spin-on dopant diffused n-type crystalline silicon solar cells *Semicond. Sci. Technol.* **31** 1–10
[21] Zanesco I, Moehlecke A, Pinto J L and Ly M 2012 Development and comparison of small and large area boron doped solar cells in n-type and p-type Cz-Si *Conf. Record of the 38th IEEE Photovoltaic Specialists Conf.* pp 2284–8
[22] Peiner E, Schlachetzki A and Kruger D 1995 Doping profile analysis in Si by electrochemical capacitance–voltage measurements *J. Electrochem. Soc.* **142** 576–80
[23] CVP21. Manual of Wafer Profiler CVP21, Electrochemical Capacitance Voltage Profiling, 2011 (http://wepcontrol.com/cv-profiler/)
[24] WT-2000PV User Manual: Measurement tool for solar cell manufacturing (http://semilab.com)
[25] Basore P A and Clugston D A 1995 PC1D Version 5: 32-bit solar cell modeling on personal computers *Conf. Record of the 26th IEEE Photovoltaic Specialists Conf.* pp 207–10
[26] Lagos R, Moehlecke A, Alonso J, Tobias I and Luque A 1994 Contamination and gettering evaluation by lifetime measurements during single crystal cell processing *Conf. Record of the First World Conf. on Photovoltaic Energy Conversion* pp 1629–32
[27] Cuevas A, Basore P A, Giroult-Matlakowski G and Dubois C 1996 Surface recombination velocity of highly doped n-type silicon *J. Appl. Phys.* **80** 3370–5
[28] Benick J, Leimenstoll A and Schultzm O 2007 Comprehensive studies of passivation quality on boron diffused silicon surfaces *Proc. 22nd European Photovoltaic Solar Energy Conf.* pp 1244–7
[29] Moehlecke A, Cañizo C, Zanesco I and Luque A 1998 Floating junction passivation of p^+ emitters *Proc. 2nd World Conf. and Exhibition on Photovoltaic Solar Energy Conversion* pp 1551–4